AD-A060 785 ROCKWELL INTERNATIONAL THOUSAND OAKS CALIF SCIENCE --ETC F/G 11/2
NONDESTRUCTIVE FAILURE PREDICTION IN CERAMICS.(U)
SEP 78 A G EVANS N00014-76-C-0624

UNCLASSIFIED SC5064-3FR NL

1 OF 1
AD
AO 60785

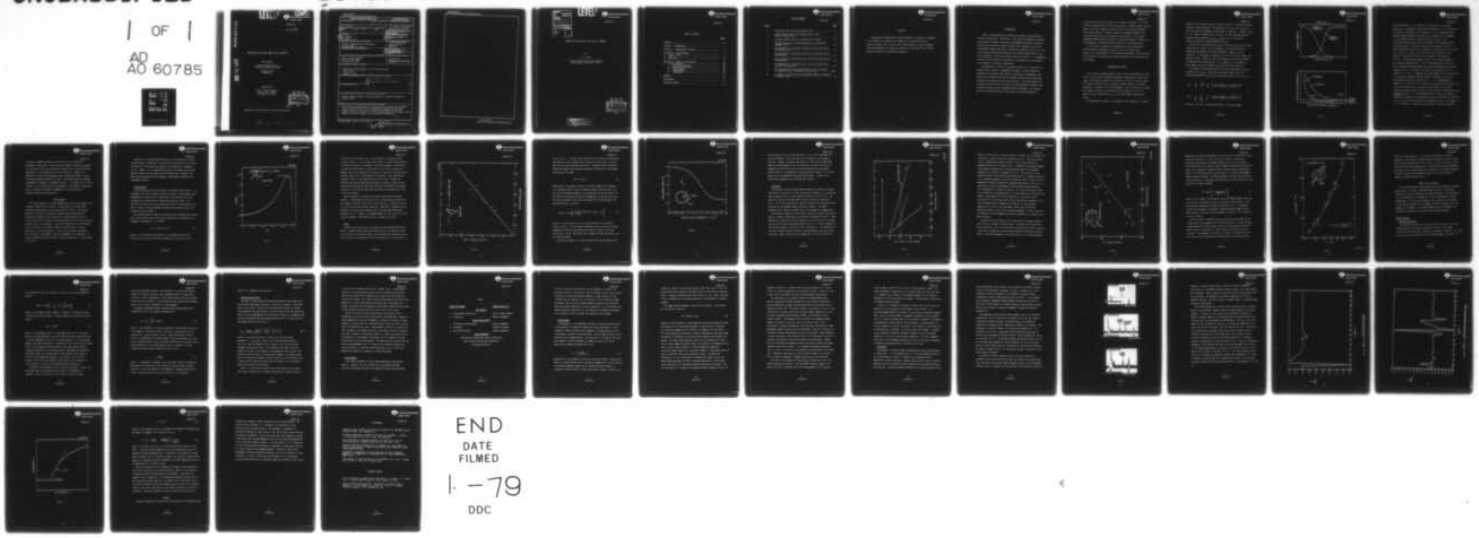

END
DATE
FILMED
1-79
DDC

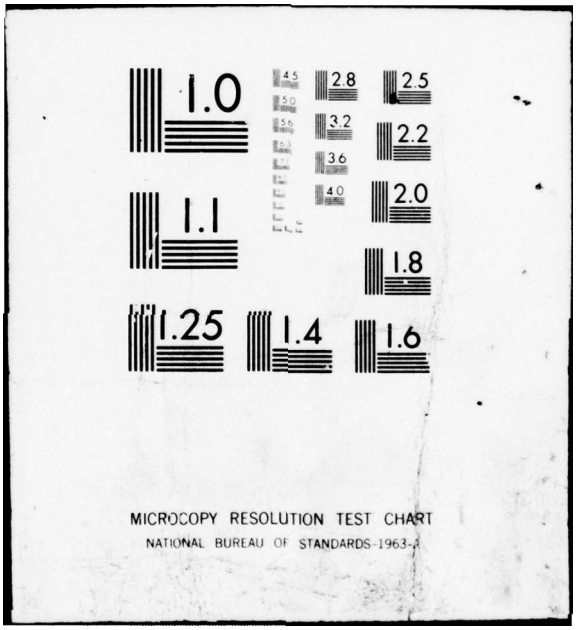
1.0
1.1
1.25
1.4
1.6
1.8
2.0
2.2
2.5
2.8
3.2
3.6
4.0
4.5
5.0
5.6
MICROCOPY RESOLUTION TEST CHART
NATIONAL BUREAU OF STANDARDS-1963-A

LEVEL II

Rockwell International
Science Center

SC5064.3FR

COPY NO. 10

AD A060785

NONDESTRUCTIVE FAILURE PREDICTION IN CERAMICS

DDC FILE COPY

Final Report

03/01/76 thru 02/28/78
Contract No. N00014-76-C-0624

Project No. 471
(NR039-129)

Submitted to:

Office of Naval Research
800 N. Quincy Street
Arlington, VA 22217

DDC
RECEIVED
NOV 3 1978
D

Approved for Public Release; distribution unlimited

78 10 26 049

UNCLASSIFIED

SECURITY CLASSIFICATION OF THIS PAGE *(When Data Entered)*

REPORT DOCUMENTATION PAGE		READ INSTRUCTIONS BEFORE COMPLETING FORM
1. REPORT NUMBER	2. GOVT ACCESSION NO.	3. RECIPIENT'S CATALOG NUMBER
4. TITLE *(and Subtitle)* (6) NONDESTRUCTIVE FAILURE PREDICTION IN CERAMICS		5. TYPE OF REPORT & PERIOD COVERED Final Report for Period 03/01/76 thru 02/28/78
		6. PERFORMING ORG. REPORT NUMBER (14) SC5064-3FR
7. AUTHOR(s) (10) A. G. EVANS		8. CONTRACT OR GRANT NUMBER(s) (15) N00014-76-C-0624
9. PERFORMING ORGANIZATION NAME AND ADDRESS Rockwell International Science Center P.O. Box 1085 Thousand Oaks, CA 91360		10. PROGRAM ELEMENT, PROJECT, TASK AREA & WORK UNIT NUMBERS Project No. 471, NR039-129
11. CONTROLLING OFFICE NAME AND ADDRESS		12. REPORT DATE (11) September 1978
		13. NUMBER OF PAGES 39
14. MONITORING AGENCY NAME & ADDRESS *(if different from Controlling Office)* Office of Naval Research 800 N. Quincy Street Arlington, VA 22217		15. SECURITY CLASS. *(of this report)* Unclassified
		15a. DECLASSIFICATION/DOWNGRADING SCHEDULE

16. DISTRIBUTION STATEMENT *(of this Report)*

Approved for Public Release; distribution unlimited.

(12) 43 p.

17. DISTRIBUTION STATEMENT *(of the abstract entered in Block 20, if different from Report)*

(9) Final rept. 1 Mar 76-28 Feb 78,

18. SUPPLEMENTARY NOTES

19. KEY WORDS *(Continue on reverse side if necessary and identify by block number)*

ceramics, NDE, ultrasonics, failure probability, rejection probability, fracture models.

20. ABSTRACT *(Continue on reverse side if necessary and identify by block number)*

Techniques for nondestructive failure prediction in ceramics are examined in the context of a probabilistic framework for obtaining failure and rejection probabilities. The ultrasonic method appears to have the greatest short-term potential for achieving acceptable failure probabilities, without the excessive rejection of satisfactory components.

DD FORM 1 JAN 73 1473 EDITION OF 1 NOV 65 IS OBSOLETE

Unclassified

SECURITY CLASSIFICATION OF THIS PAGE *(When Data Entered)*

389 949

ACCESSION for
NTIS White Section
DDC Buff Section
UNANNOUNCED
JUSTIFICATION
BY
DISTRIBUTION/AVAILABILITY CODES
Dist. AVAIL. and/or SPECIAL
A

LEVEL II

Rockwell International
Science Center

SC5064.3FR

NONDESTRUCTIVE FAILURE PREDICTION IN CERAMICS

By

A. G. Evans

Rockwell International Science Center
Thousand Oaks, California 91360

DDC
RECEIVED
NOV 3 1978
D

DISTRIBUTION STATEMENT A
Approved for public release;
Distribution Unlimited

TABLE OF CONTENTS

	Page
ABSTRACT	iii
SECTION I - INTRODUCTION	1
SECTION II - ACCEPT/REJECT CRITERIA	2
SECTION III - FAILURE MODELS	6
A. Surface Cracks	7
B. Voids	9
C. Inclusions	13
SECTION III - DEFECT SIZE ESTIMATION	19
A. Indirect Methods	19
1. Statistical Analysis	19
2. Overload Proof Testing	22
3. Direct Methods	23
4. X-Radiography	25
5. Ultrasonics	28
SUMMARY	35
BIBLIOGRAPHY	37
TECHNICAL REPORTS	37

LIST OF FIGURES

Figure		Page
1	False-accept and false-reject probabilities.....	4
2	Stress intensity factor distribution around a semi-circular surface crack.....	8
3	Fracture prediction data for surface cracks in glass.....	10
4	Fracture from voids in brittle materials; the distribution parameter, $D(\alpha)$.....	12
5	The dependence of the fracture strength of silicon nitride on the inclusion size.....	14
6	The correlation of the fracture data for Si inclusions with the fracture model.....	16
7	The correlation of the fracture data for Fe inclusions with the fracture model.....	18
8	The detectability of surface cracks in silicon nitride using ultrasonic surface waves.....	30
9	The calculated scattering characteristics in the time domain (a) spherical void, (b) spherical WC inclusion.....	32/33
10	A schematic indicating the long wavelength method for estimating the defect volume.....	34

ABSTRACT

Techniques for nondestructive failure prediction in ceramics are examined in the context of a probabilistic framework for obtaining failure and rejection probabilities. The ultrasonic method appears to have the greatest short-term potential for achieving acceptable failure probabilities, without excessive rejection of satisfactory components.

INTRODUCTION

Several unique properties of ceramics are presently being exploited in structural applications. Specifically, their good high temperature strength and oxidation (corrosion) resistance has engendered considerable interest in ceramic energy conversion systems (turbines, heat exchangers), while their high hardness renders them uniquely applicable to bearings, valves, etc. One of the primary problems associated with the structural application of such brittle materials is their wide fracture strength variability. In consequence, effective failure prediction techniques are a prerequisite to the reliable use of ceramics in structural applications.

The prediction of failure in structural ceramics can, in principle, be achieved using a number of independent techniques. The most extensively developed are the direct defect detection techniques (x-radiography, penetrants, and ultrasonics) and the flaw strength characterization techniques (overload proof testing and statistical analysis). Many other methods are available as possible (but less likely) failure prediction candidates; some of these are based on quite independent physical phenomena, e.g. acoustic emission, exo-electron emission, while others are alternate methods of

visualizing similar physical effects, e.g. acoustic holography. All of the available techniques have limitations when applied to ceramic systems, and one method is unlikely to emerge as the universal failure prediction approach. The pertinent method will probably depend on the component geometry, the in-service stress state, and the material microstructure. Also, several independent techniques may be required to assure the structural integrity of a given component, without the excessive rejection of satisfactory parts.

In this review, an approach for nondestructive failure prediction in ceramic systems is developed, to provide a basis for assessing the capabilities of the potential failure prediction approaches. Then, the merits and limitations of the principal avialable techniques for failure prediction are reviewed.

ACCEPT/REJECT CRITERIA

The fracture of ceramics generally occurs by the direct extension of small cracks in the vicinity of pre-existing defects; these defects include large pores, inclusions and large grains (frequently as sites for machining flaws). The fracture condition is not, in general, related uniquely to the defect dimensions. A probability of fracture $\phi(\sigma_\infty^c/a,b,c)$ must, therefore, be assigned to a defect of given size (with three principal dimensions a,b,c) for a specific level of applied stress σ_∞ in the volume element containing the defect .

The nondestructive capability for determining the dimensions of a defect

depends on the inspection method; invariably, an error is associated with the estimate of these dimensions. The magnitude of the error and its specific form are sensitively dependent on the method of inspection. In general, there will be a specific probability, e.g. $\phi(a_{es}/a)$, for each technique that the estimated defect dimensions (a_{es}, b_{es}, c_{es}) will be in a certain size range, given the actual defect dimensions (a,b,c).

We have thus far identified two probabilities: one concering the fracture probability for a defect of given dimensions, the other concering the nondestructive estimate of the defect dimensions. However, a third probability is also needed to complete the reliability analysis; namely, the probability that a defect in a given size range will exist in the volume of the component being inspected, $\Phi(a)$. This probability is estimated by metallographic studies on samples taken from each batch of material.

The product of these three probabilities can be integrated to various inspection levels, a^*_{es}, to obtain two interrelated probabilities: the false-accept probability Φ_A and the false-reject probability Φ_R (Fig. 1a):

$$\Phi_A = \int_0^{\sigma_A} \int_0^{a^*_{es}} \int_0^{\infty} \left[\phi(\sigma^c_\infty/a)\,d\sigma_\infty\right]\left[\phi(a_{es}/a)\,da_{es}\right]\left[\phi(a)\,da\right] \tag{1}$$

$$\Phi_R = \int_{\sigma_A}^{\infty} \int_{a^*_{es}}^{\infty} \int_0^{\infty} \left[\phi(\sigma^c_\infty/a)\,d\sigma_\infty\right]\left[\phi(a_{es}/a)\,da_{es}\right]\left[\phi(a)\,da\right]$$

where σ_A is the level of the applied tension in the volume element

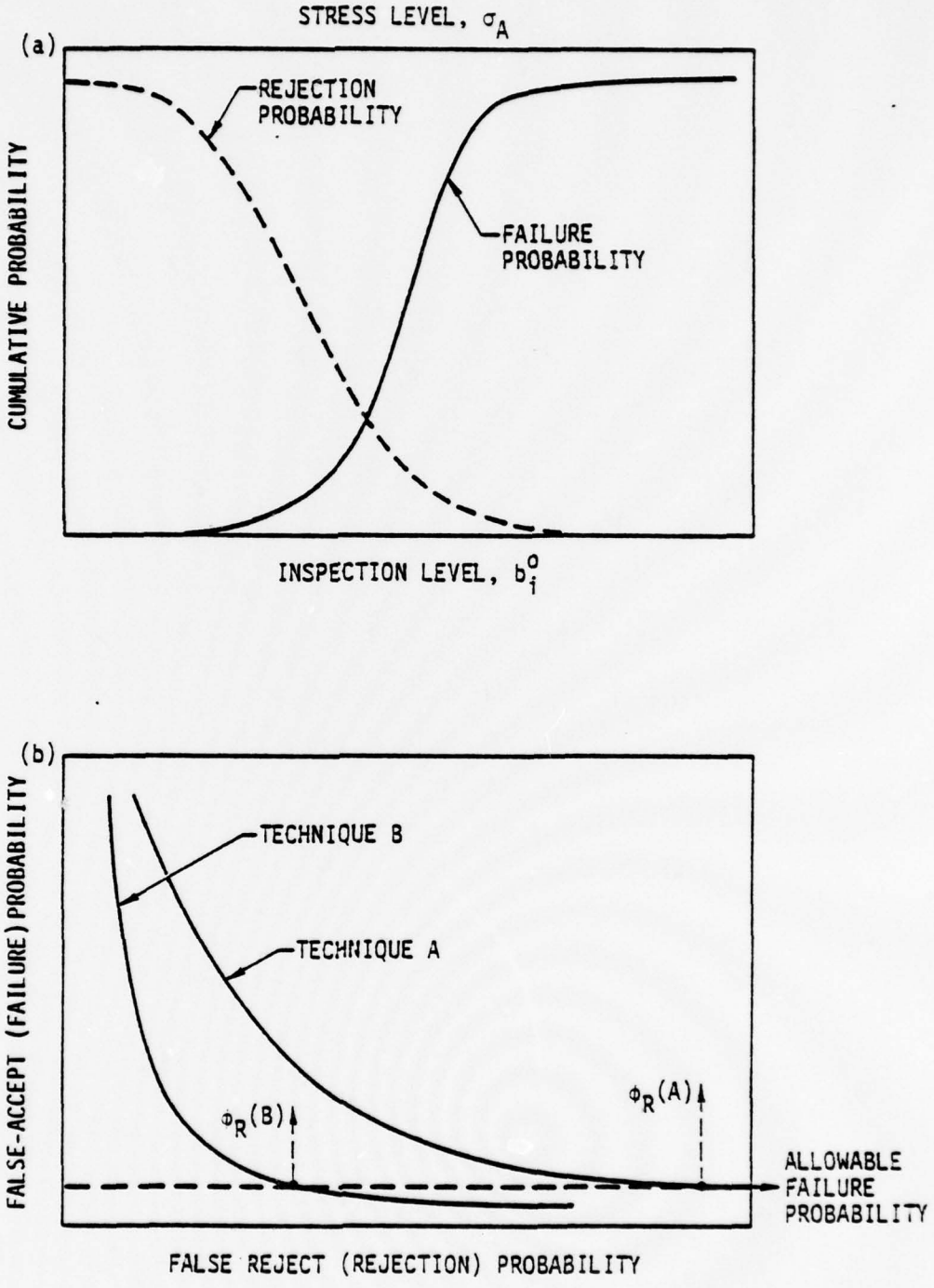
STRESS LEVEL, σ_A
(a)
REJECTION PROBABILITY
FAILURE PROBABILITY
CUMULATIVE PROBABILITY
INSPECTION LEVEL, b_i^o
(b)
TECHNIQUE B
TECHNIQUE A
$\Phi_R(B)$
$\Phi_R(A)$
ALLOWABLE FAILURE PROBABILITY
FALSE-ACCEPT (FAILURE) PROBABILITY
FALSE REJECT (REJECTION) PROBABILITY

Figure 1

containing the defect. The inspection level a_{es}^* refers to the defect dimension(s), as estimated by the inspection technique, that is selected for the rejection or acceptance of the component, e.g. all components with an estimated maximum dimension less than a_{es}^* are accepted and all components with an estimated dimension greater than a_{es}^* are rejected. The false-accept probability Φ_A is thus the probability that components that have been accepted, in accord with the specified inspection level, will contain defects more severe than indicated by the estimate, and will actually fail in service, i.e. Φ_A is the in-service failure probability. This probability decreases, of course, as the inspection level decreases (Fig. 1a). The false-reject probability Φ_R is the (related) probability that rejected components would, in fact, have performed satisfactorily in service, because the defect severity has been overestimated by the selected inspection level. This probility increases as a_{es}^* decreases (Fig. 1a). However, it is crucial to recognize that these probabilities are interrelated, i.e. they merely represent different ranges of integration of the same combination of probability functions (Eq. 1). This interdependence is exemplified in Fig. 1b, which is a typical plot relating the false-accept and false-reject probabilities - once one of these probabilities has been selected, the other probability as well as the associated inspection level are necessarily defined. It is now apparent from Fig. 1b that the inspection technique, or combination of techniques, that would be preferred is that which yields a curve as close as possible to the probability axes. For example, in Fig. 1b, technique B is preferred over technique A, because the rejection of

satisfactory components required to satisfy the failure probability requirement is much lower. Such curves thus represent a quantitative method for characterizing the failure prediction capabilities of various inspection techniques, for a given material and service condition. However, the generation of these curves represents a major experimental effort, and the information presently available is limited. The present status and imminent developments are examined in subsequent sections. It is hoped that all future studies will be directed toward the development of false-accept, false-reject curves, to enable a quantitative framework for failure prediction in structural ceramics to be constructed.

FAILURE MODELS

The fracture process in a ceramic depends specifically on the material and the defect responsible for fracture. In most materials, surface cracks introduced by machining are a consistent source of failure. This failure mechanism is particularly prevalent in dense, coarse grained materials. Inclusions introduced during fabrication are another prominent origin of failure, particularly in dense, fine grained materials (for which failure from surface cracks is less dominant). Individual large pores, or a concentrated array of fine pores, are another frequently observed source of failure, particularly in sintered materials. Finally, surface cracks introduced by post fabrication, environmental interaction phenomena can be important, i.e. cracks introduced by projectile impact, contact stresses etc. or cracks formed by oxidation.

Probablistic information concerning these failure processes is limited. The most extensive information is available for hot pressed silicon nitride. This material is thus used as an example of the probablistic treatment of failure. However, it is re-emphasized that the failure model can be highly specific, both to the host material and the defect type. Therefore, the models described should only be extended to other materials/defects with considerable caution.

Surface Cracks

The surface crack has been the subject of extensive recent analysis. In consequence, the stress intensity factor distribution is now relatively well comprehended for semi-circular cracks normal to the surface (Fig. 2) and reasonably well-characterized for normal semi-elliptical cracks. The equivalent solutions for cracks at other inclinations to the surface are not known in detail; although reasonable estimates can be based on results for contained elliptical cracks.

One possible model of fracture from surface cracks considers that fracture occurs when the peak value of the stress intensity factor reaches the local toughness of the material, K_c, yielding;

$$\sigma_f = Z\ (a/c, \theta)\ K_c\ a^{-\frac{1}{2}} \qquad (2)$$

where σ_f is the fracture stress measured in the absence of slow crack growth, a and c are the two principal dimensions of the crack, θ is its

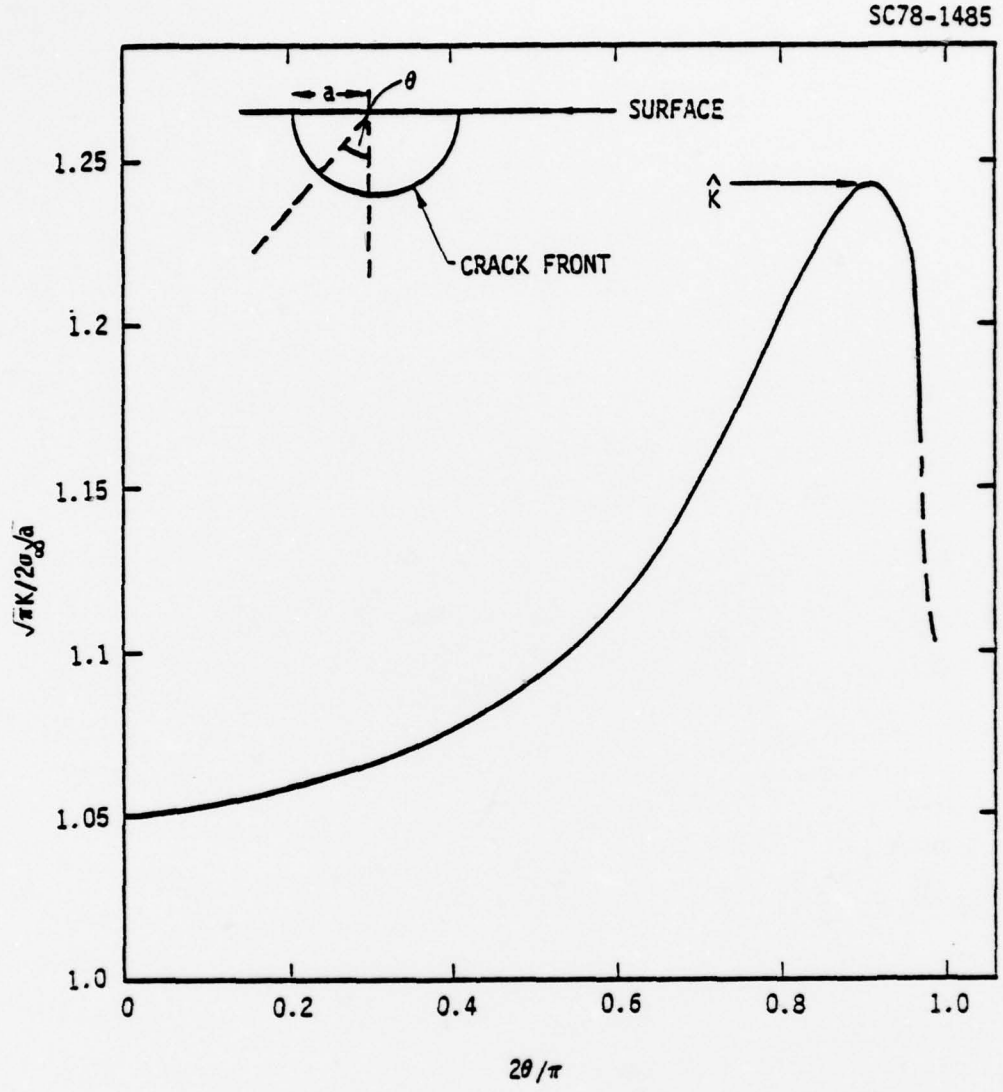
SC78-1485
a
θ
SURFACE
CRACK FRONT
K̂
1.25
1.2
1.15
1.1
1.05
1.0
0
0.2
0.4
0.6
0.8
1.0
√πK/2σ_s√a
2θ/π

Figure 2

inclination to the surface, and Z is the analytically determined stress intensity function. For this model, the variability in the fracture stress is attributed exclusively to variations in the local toughness: distributions in σ_f ($\phi(\sigma_f/a,c,\theta)$) pertinent to such variability are likely to be Gaussian. However, sub-critical extension of the crack in a region of high local stress intensity factor (Fig. 2) may precede final fracture. Then, there may be systematic trends in the fracture stress with a/c and θ. Probability functions that neglect these possible trends will exhibit a wider and less characteristic distribution than those that take these effects into account. The details of the fracture model thus constitutes an important part of the reliability analysis.

Specific probability functions for surface cracks have not yet been obtained, largely because of the difficulty in distinguishing the profile of the fracture initiating crack on the fracture surface. A viable solution to this difficulty has not yet been identified. Some useful information can be obtained by introducing well-defined cracks using the Knoop indentation technique (Fig. 3). However, this method samples only the variability in the fracture toughness. Much additional work is needed in this area.

Voids

Fracture from isolated voids in ceramics has been analyzed using several models. The model which accounts most effectively for the observed trends with void size is a statistical model, which considers that fracture occurs by the activation of a distribution of flaws that pre-exist in the vicinity of

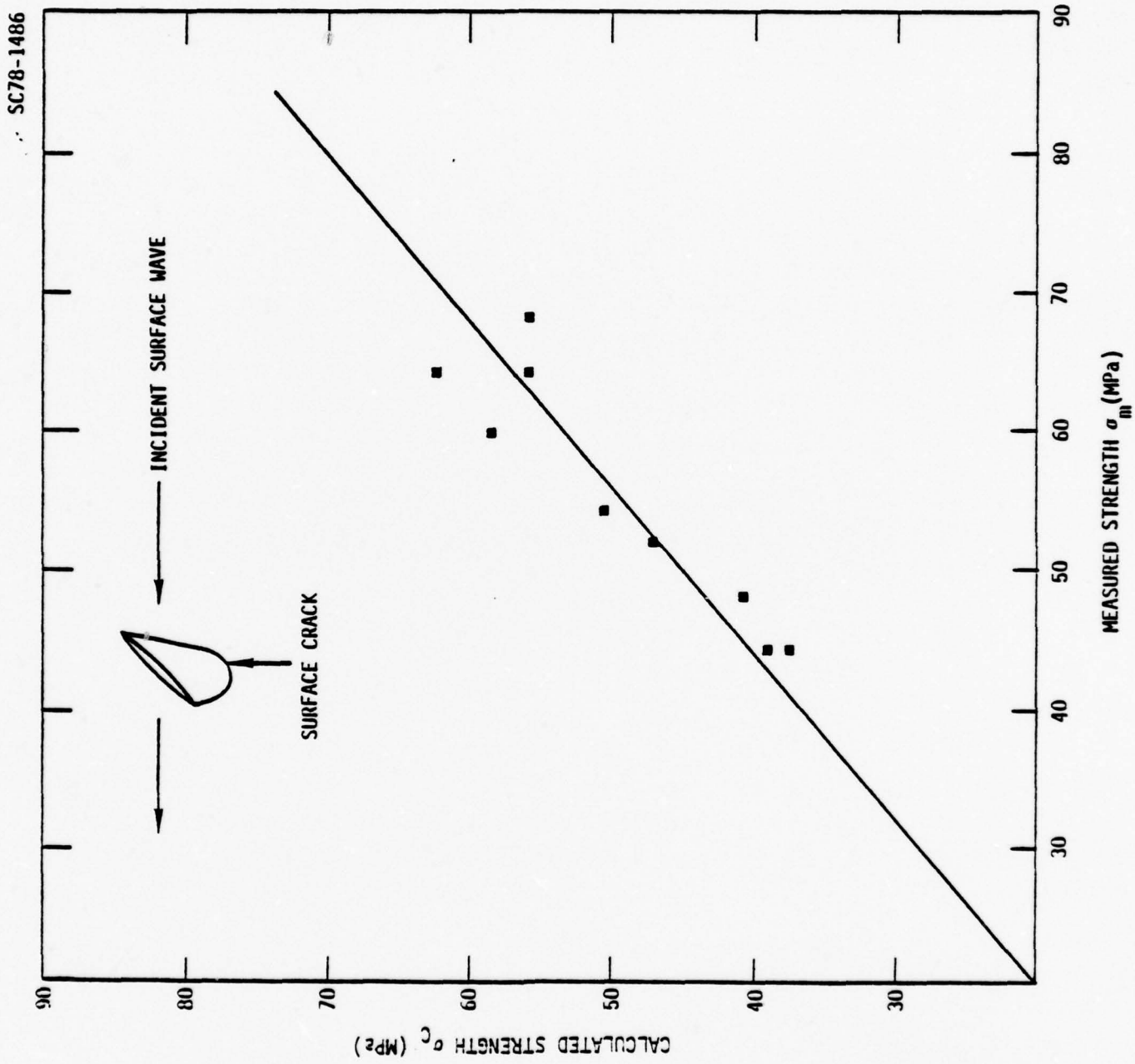
SC78-1486
INCIDENT SURFACE WAVE
SURFACE CRACK
CALCULATED STRENGTH σ_c (MPa)
MEASURED STRENGTH σ_m (MPa)
90
80
70
60
50
40
30

Figure 3

the void (Fig. 1). The most likely fracture initiating flaws are microcracks associated with grain boundary cusps on the void surface (small inclusions near the void are an alternate possibility). Analyses of both surface and volume distributed flaws have been conducted by considering a flaw strength distribution of the type

$$g(S) = \lambda (S/S_o)^k \tag{3}$$

where $g(S)dS$ is the number of flaws in unit area (volume) with a strength (i.e. extension stress in uniaxial tension) between S and S+dS, and λ, S_o and k are distribution parameters to be determined from the test data. For the surface flaw problem, the analysis encompasses all possible flaw sizes, and yields the general result that the probability of fracture $\Phi(\sigma_\infty^c)$ at an applied stress σ_∞^c is given by;

$$\Phi(\sigma_\infty^c) = 1-\exp\left[8\lambda r^2 \left(\frac{\sigma_\infty^c}{S_o}\right)^k D^k(\alpha) \exp(0.52k - 0.14)\right] \tag{4}$$

where r is the void radius, $\alpha = (1/r)(K_c/S_o)^2$ and $D(\alpha)$ is the function plotted in Fig. 4. For the volume flaw problem, the analysis has only been conducted for flaws very much smaller than the void radius, and is thus restricted in utility. Additional work is needed to extend the analysis into the large flaw regime.

A considerable quantity of fracture data are required to determine the

SC78-1487

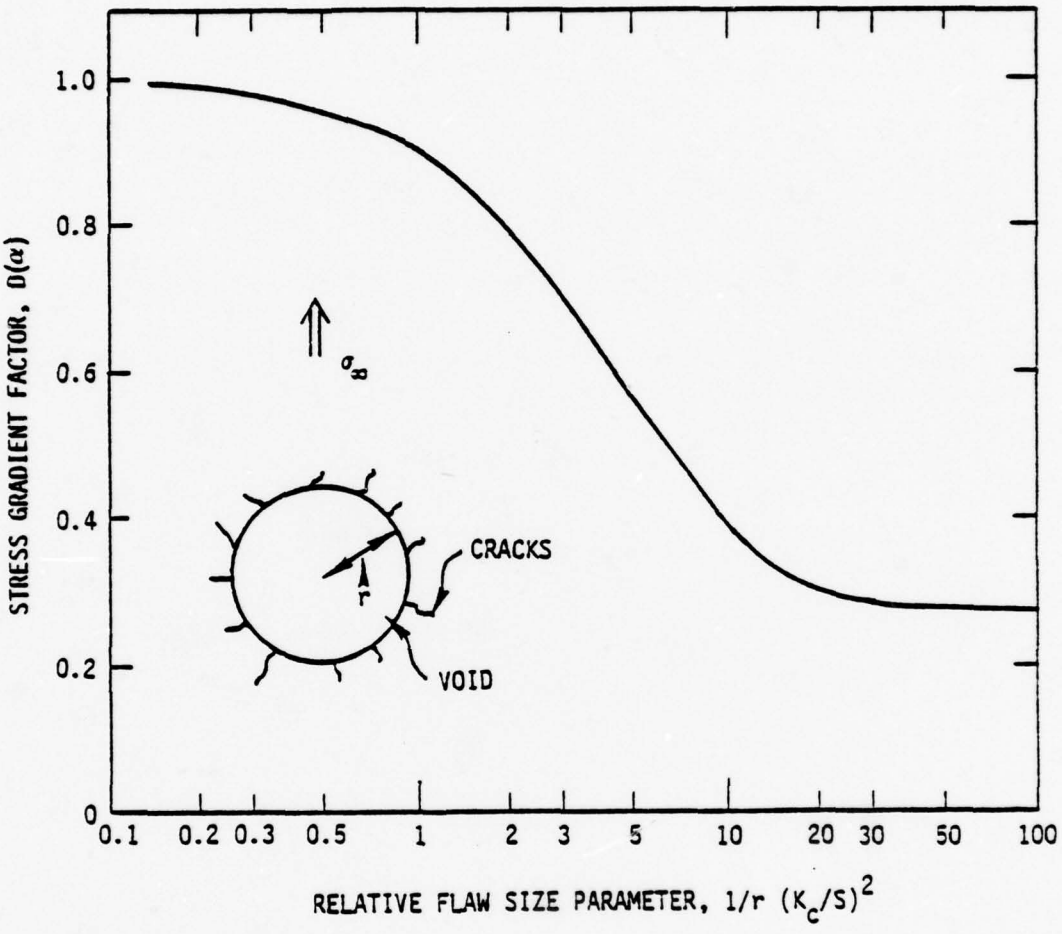

Figure 4

detailed applicability of the surface model vis-a-vis the volume model for a particular material. Sufficient data for this purpose are not presently available. However, the general pertinence of a statistically based model seems to be substantiated by the available data, particularly by the size dependence of the fracture stress at constant probability: other models predict either no size dependence (stress concentration model) or on inverse square root size dependence (crack equivalence models). Values of the distribution parameters can be obtained from the data.

Inclusions

The pertinent inclusion fracture model depends on the specific inclusion. Three types of inclusions in silicon nitride are considered, to illustrate the range of possibilities: silicon, tungsten carbide, and iron silicide. The trends with inclusion size obtained for these inclusions are depicted in Fig. 5. The silicon inclusion has a strong influence on the strength; whereas the effect of the tungsten carbide inclusion is minimal. The need to nondestructively identify the defect type is thus dramatically demonstrated.

Post-fracture inspection of the silicon inclusions indicates that they are dense, i.e. contain little porosity, and exhibit transgranular fracture. These observations, coupled with the low toughness of silicon (0.6 MPa$\sqrt{m}$), suggest that the silicon inclusions fracture sub-critically, i.e. without propagating into the much tougher (5 MPa $\sqrt{m}$) silicon nitride matrix. This expectation is verified by acoustic emission studies on stressed samples containing silicon inclusions. Hence, since the elastic properties of silicon are similar to

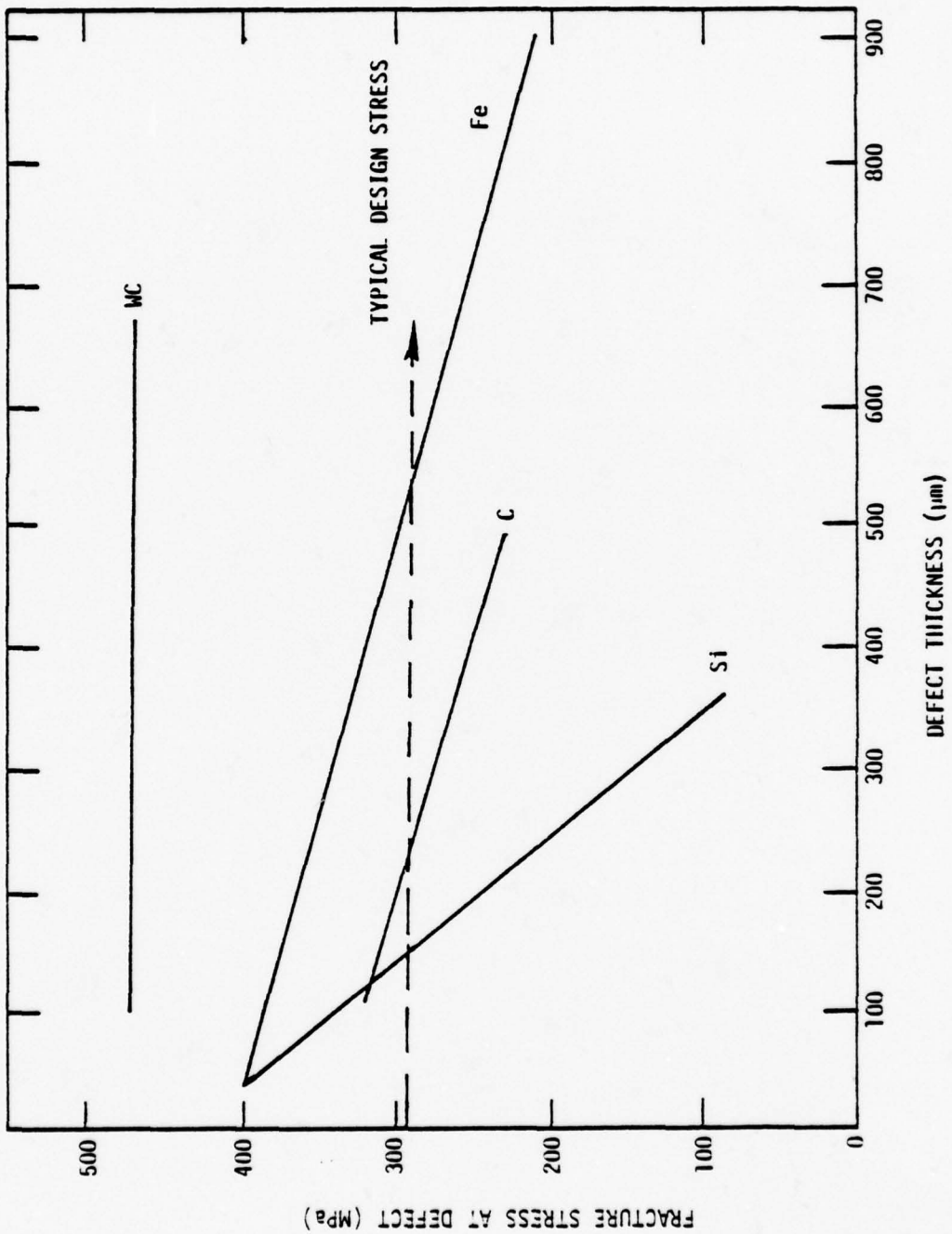
TYPICAL DESIGN STRESS
WC
Fe
C
Si
FRACTURE STRESS AT DEFECT (MPa)
DEFECT THICKNESS (μm)
500
400
300
200
100
0
100
200
300
400
500
600
700
800
900

Figure 5

those of silicon nitride, a plausible model of ultimate fracture considers the inclusions as cracks of equivalent dimensions (Fig. 6). Then, the fracture stress is governed by an equation similar to Eq.(2) that contains the appropriate Z(a/c) for an internal crack. A comparison of measured strengths with strengths predicted by the crack equivalence model for an assumed toughness K_c of 5 MPa$\sqrt{m}$ is presented in Fig. 6. The variability in the measured fracture stress might be attributed either to a toughness variability or to a combined toughness, sub-critical extension effect. The data are not comprehensive enough to unequivocally separate these possibilities. but it is noted that the ratio of the measured to the predicted strength exhibits a close conformance to a normal distribution. This type of distribution would be anticipated for the toughness when, as in the present case, the crack front samples a large number of silicon nitride grains. The center of this distribution at 0.8 indicates either that the average local toughness is less then the assumed value (4 compared with 5 MPa$\sqrt{m}$), or that the crack dimensions at criticality are consistently larger than the inclusion dimensions, because of sub-critical extension phenomena. Finally, note that the important inclusion dimensions are the two dimensions (a,c) normal to the applied tension.

Inspection of the fractured iron silicide inclusions indicates extensive porosity and an irregular fracture surface. A different fracture mechanism might thus pertain. This is verified when the above fracture model is applied to test data; the measured strengths greatly exceed the predicted values and exhibit a diminished dependence on the inclusion size. An alternative model

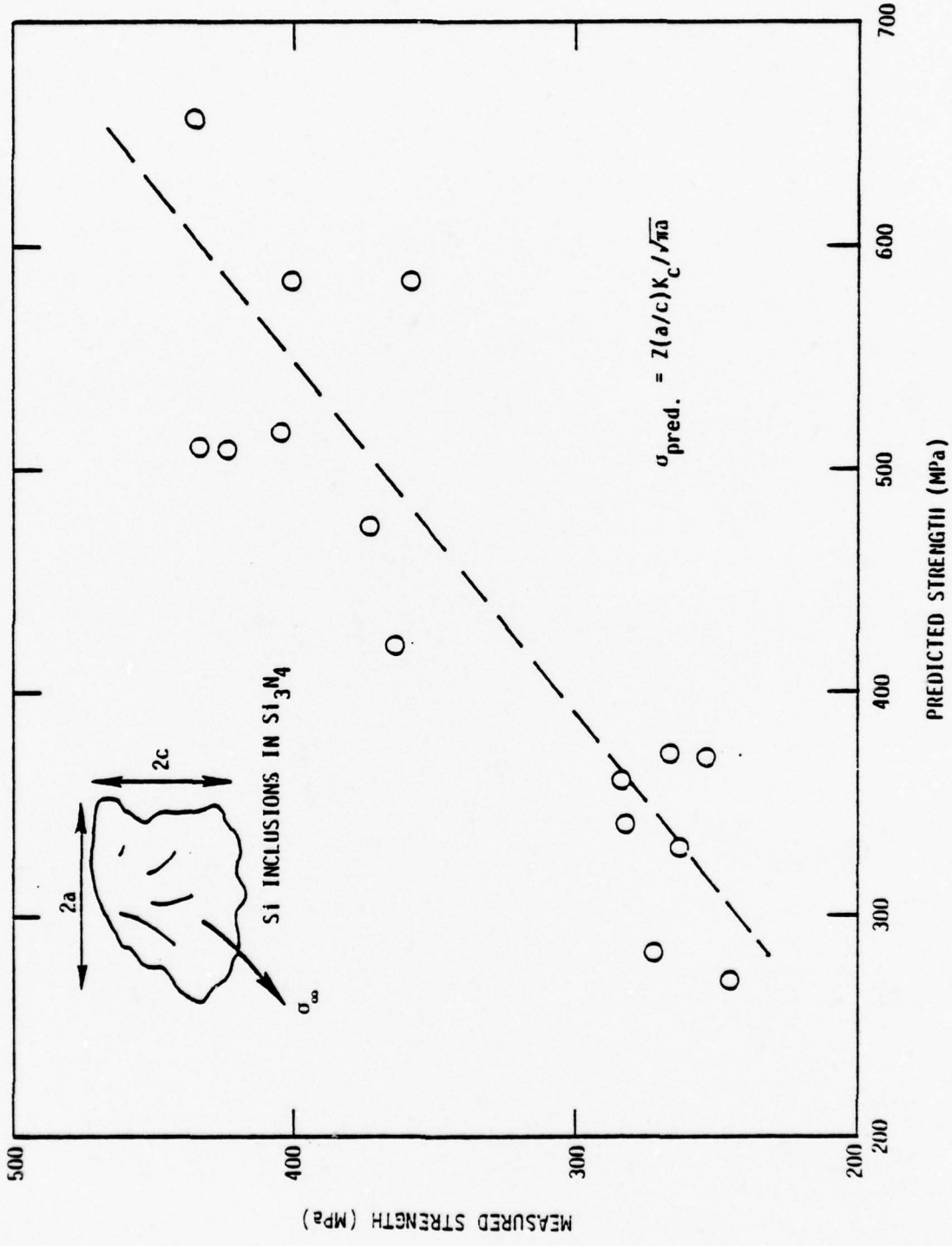
MEASURED STRENGTH (MPa)
PREDICTED STRENGTH (MPa)
500
400
300
200
700
600
500
400
300
200
$\sigma_{pred.} = Y(a/c)K_c/\sqrt{\pi a}$
Si INCLUSIONS IN Si_3N_4
2a
2c
σ_a

Figure 6

suggested by the fracture morphology is that fracture initiates from the pores within the inclusions, i.e. the inclusion is treated as a porous body subjected to the stress field imposed through the silicon nitride matrix. This stress field is the result of thermal expansion mismatch and the applied stress. For ellipsoidal inclusions, both of these stresses are hydrostatic (equal in all three directions), and the analysis of fracture then becomes a simple statistical problem. Analyzing the porous inclusion using statistical flaw distributions, in the manner described above for fracture from voids, the probability of fracture becomes

$$\Phi = 1-\exp\left[-V\left(\frac{\beta\sigma_\infty + \sigma_\alpha}{S_0}\right)^k\right] \qquad (5)$$

where V is the volume of the inclusion, σ_α is the thermal mismatch stress and β is the ratio of the applied stress to the stress in the inclusion. Test data analyzed according to this model are plotted in Fig. 7. Reasonable values of the parameters are obtained, indicating that the model has merit. Note, therefore, that the inclusion parameter of interest in this instance is its total volume, V.

The minor effect of tungsten carbide inclusions on the strength derives from both their high toughness and large elastic modulus. The high toughness prevents premature inclusion fracture, while the large modulus confines the zone of tension in the matrix to a small region around the poles of the inclusion. In consequence, the statistical analysis of fracture from this small zone of tension indicates low fracture probabilities at appreciable

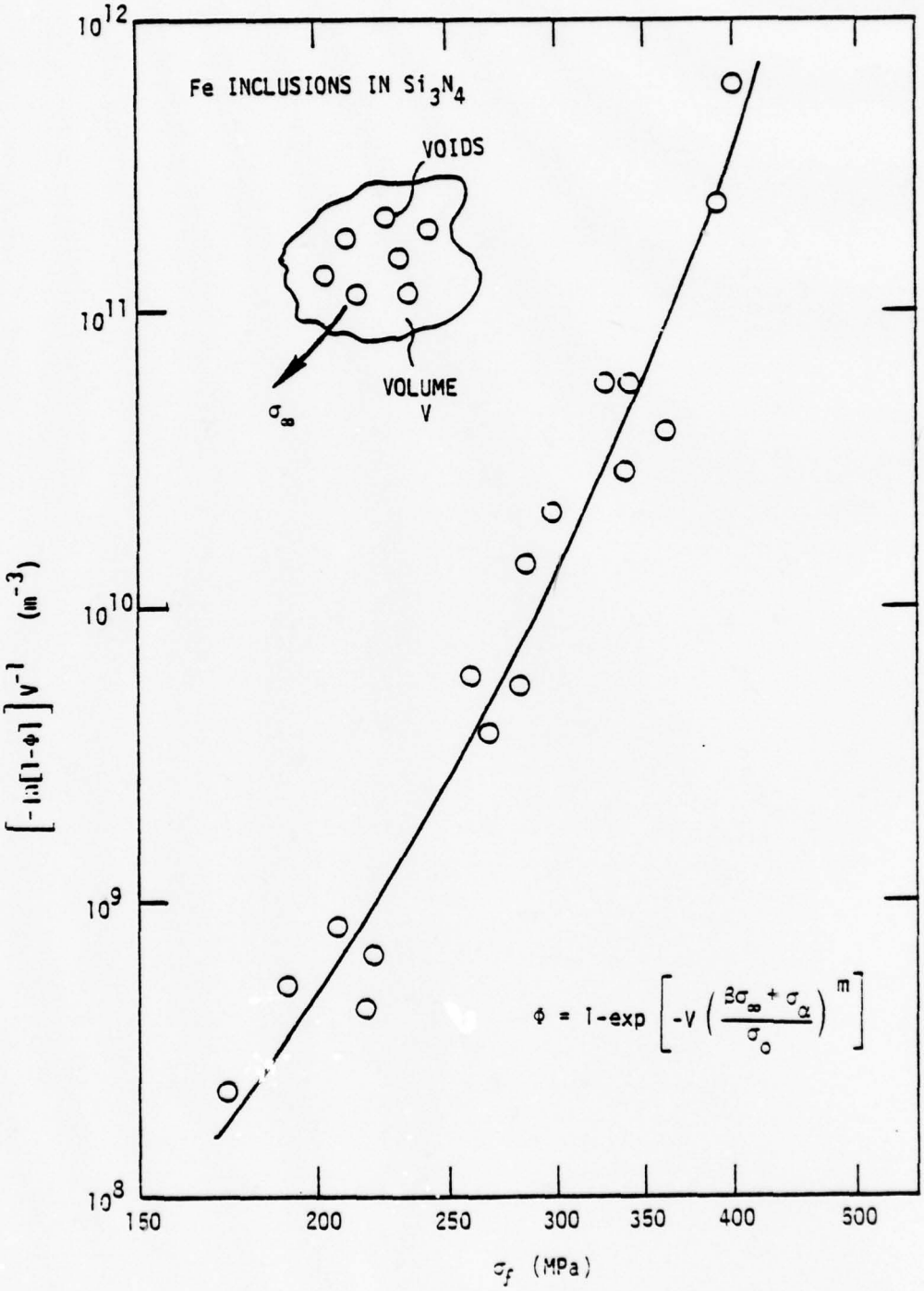

SC78-1227

Figure 7

levels of the applied stress. In qualitative confirmation of these expectations, the fracture of samples containing tungsten carbide inclusions usually occurs from small matrix voids in the vicinity of the poles. There are not yet sufficient fracture data to identify the distribution parameters pertinent to this fracture process; but, tentatively, the fracture probability for these inclusions can be equated to zero, for the stress levels of practical interest, $\lesssim 300$ MPa (Fig. 5).

DEFECT SIZE ESTIMATION

It is apparent from the fracture models that greatly reduced false-reject probabilities will result if the defect type, as well as its pertinent dimension(s), can be elucidated by the inspection method. This requirement is a vital consideration in the comparison of the various methods of defect determination. This particular problem is not a concern for the indirect failure prediction method, which estimates the defect 'strength'; but other problems are introduced. The indirect methods are thus considered first, followed by a discussion of the direct defect detection methods.

Indirect Methods

Statistical Analysis

The statistical prediction of failure relies on an ability to directly characterize the flaw strength distribution function. The strength distribution function $g(S)dS$ is defined as the number of flaws per unit volume (or unit area for surface flaws) with a strength between S and S+dS. For

non-interacting flaws, this function is related to the fracture probability $\Phi(S)$ by

$$\Phi(S) = 1 - \exp\left[- \int_{V_o} dV_o \int_o^S g(S)dS \right] \tag{6}$$

where V_o is the sample volume. Recently, a method for obtaining g(S) from fracture data has been devised. A typical example, which applies to tensile tests is

$$g(S) = \xi'/\pi r^2 \ell \tag{7}$$

where r is the specimen radius, ℓ is the gauge length, and $\xi = -\ell n(1-\Phi(S))$. Once g(S) has been obtained in this way, within the stress range that exists in the test component, Eq.(6) can be evaluated numerically for any specimen geometry and stress distribution. The constraint that the test data pertinent to low failure probabilities be obtained in the stress range of concern (because extrapolation to low stresses cannot be performed with appreciable confidence) means, for most applications, that extensive tensile data on relatively large samples are required. (By contrast, the low failure probabilities for the direct methods relate primarily to the probability, $\phi(a)da$ (see Eqn. 1), which can be determined metallographically.)

The method in its present form has an additional weakness - notably, the requirement that the flaw population be invariant from component to component. Such an invariance is quite unlikely for typical ceramic

fabrication processes and hence, high confidence in the predicted fracture probability cannot be achieved. Some independent method for identifying variations in the flaw population is thus required before statistical methods can be realistically applied. Such a possibility has recently been proposed, based on the ultrasonic attenuation α of the component.

Ultrasonic attenuation affords a measure of the large extreme of the microstructure, or of the surface crack population;

$$\alpha(f) = \frac{1}{2} \int_0^\infty \Omega(r,f) g(r) dr \tag{8}$$

where f is the frequency, Ω is the cross section of the scatterer, and g(r)dr is the number of large grains (pores, inclusions, surface cracks) per unit volume (area) in the size range r to r+dr. Hence for materials in which fracture is determined by the large extreme of the microstructure (e.g. large pores in reaction bonded silicon nitride and large grains in relatively coarse grained materials), or by surface cracks, g(r)dr is related to the flaw strength distribution g(S)dS through the usual relation

$$S = \frac{K_c}{Y\sqrt{r}} \tag{9}$$

where Y is a parameter that depends on the flaw shape. Hence, an attenuation measurement could define g(S)dS and thereby the fracture probability $\Phi(S)$. Variability in the flaw population from component to component might thus be directly incorporated into the failure prediction. This intriguing

possibility is presently being explored.

Overload Proof Testing

The theory of proof testing has been established for several years, but the pertinent experimental evaluation is only now in progress. The present status is as follows. The utility of overload proof testing to eliminate those components that would normally fail during service has been established theoretically and experimentally for proof tests conducted in an ambience that excludes significant slow crack growth during the test. For such conditions the minimum time to failure, t_{min}, is

$$t_{min} = \frac{2}{(n-2)v_o} \left(\frac{K_c}{\sigma_a Y}\right)^2 \left(\frac{K_o}{K_c}\right)^n \left[R^{n-2}-1\right] \qquad (10)$$

where R is the proof ratio and n, v_o and K_o are slow crack growth parameters ($v = v_o(K/K_o)^n$). There is also a well-defined variance of the failure time that depends on the variances in the slow crack growth parameters and the proof ratio. This minimum failure time is realized whenever the stress in each element of the component during the proof test exceeds the service stress (in the equivalent element) by an amount greater than R; provided that extraneous interface stresses are not developed during unloading and that additional defects are not produced (e.g. by projectile impact and oxidation) during service.

When it is not possible to exclude slow crack growth during the proof test, theory indicates that a minimum unloading time is needed to assure a

finite survival time after proof testing. However, even if this minimum is impractical, the theory predicts that the failure probability after proof testing can be many orders of magnitude less than the failure probability without proof testing. This latter effect has been observed, but the failure probability is often larger than the predicted value. This disparity is probably associated with the presence of crack growth instabilities that occur during unloading at stress intensities close to the critical value.

Another restriction of proof testing concerns the practicality of reproducing the in-service stress distribution in the proof test. Except for simple geometries or service environments, a substantial fraction of volume elements in the proof test will experience stress ratios that differ from the ideal value specified by Eq.(10). Those elements for which R is smaller than ideal introduce a false-accept probability, and those for which R is greater than ideal introduces a false-reject probability. Hence, each proof test can be expressed as a false-accept, false-reject curve for comparison with the curves derived for the direct methods. This quantification of proof tests has not yet been implemented, but it is urged that this method of gauging the relative efficacy of a particular proof test design, vis-a-vis the direct nondestructive methods, be adopted as a future requirement.

Direct Methods

A wide range of methods for direct defect detection has been devised (Table I). However, only the ultrasonic and x-ray methods have been sufficiently developed that some of the important issues concerning defect

TABLE I

INSPECTION METHODS	PRIMARY SENSITIVITY
BULK DEFECTS	
1. X-Radiography (Microfocus)	Density (Atomic Number)
2. Ultrasonics	Acoustic Impedance
NEAR SURFACE DEFECTS	
1. Ultrasonics (Surface Waves)	Acoustic Impedence
2. Microwaves	Dielectric Constant
3. Acoustic Microscopy	Acoustic Impedance
NOVEL APPROACHES	
Photo-Acoustic Spectroscopy (Optical Absorption)	
Eddy Currents (Space Charge Interaction)	
Exo-Electron Emission	

distinction and size characterization can be adequately discussed. The detailed dicussion is restricted to these two methods, but this should not be construed to indicate that the other methods, as they develop, will not ultimately play an important role in the overall failure prediction scheme. For example, the ability of microwave methods to detect silicon inclusions might be of great significance in failure prediction in silicon nitride; also, improved penetrant techniques (e.g. dye enhanced x-ray methods) may perhaps find an important niche in surface crack characterization schemes.

X-Radiography

X-radiography is a well-developed technique, and the principles involved in the generation of images from defects are largely understood. A brief statement of these principles allows judgments to be made about the role of X-radiography in ceramic failure prediction. The two image variables are the resolution and the image contrast. The resolution χ is related to the focal spot diameter f, and the distances d_1, between the focal point and the defect and d_2, between the defect and film by

$$\chi = f\left(\frac{d_2}{d_1 + d_2}\right) . \qquad (11)$$

Conventional x-ray equipment utilizes focal spot tubes $\geq 500\mu m$ in diameter and hence, for typical dispositions of the source, component and film (as realized for nonsimple component geometries) the maximum resolution ($\geq 100\mu m$) is inadequate for most structural ceramic applications. However, refined x-ray

systems are capable of achieving much smaller focal spot sizes; in fact, the Cosslett-Nixon type projection instrument (which utilizes electron focussing tubes) is capable of producing spot sizes as small as ~1μm. Hence, resolution is not a limitation per se to the application of X-radiography to structural ceramics.

The image contrast represents a more serious limitation. The contrast, ΔI, on the film is given by

$$\Delta I = 0.86 \Delta\mu \; a\gamma_D/\beta \qquad (12)$$

where $\Delta\mu$ is the difference in linear absorption coefficient between the defect and the matrix, 2a is the defect thickness (in the direction of the beam), γ_D is the x-ray "gamma" of the film and β is a numerical build-up factor. The linear absorption coefficient is primarily determined by the atomic number and density of the material and varies with the energy of the incident x-ray photons. The atomic number/density relation for the elements with closely similar atomic numbers can exhibit large x-ray absorption differences and vice versa. Certain types of defects will thus be capable of generating significant image contrast for a given matrix material; these defect types can often be predicted from available absorption tables. The absorption differential, $\Delta\mu$, for a given defect increases quite rapidly as the x-ray photon energy decreases and hence, to maximize detectability, the minimum energy consistent with a practicable exposure time should be selected. The build-up factor, β, increases as the sample thickness increases and thus, the

component thickness is a variable effecting defect detectability. Finally, since ΔI is directly proportional to the defect thickness a, there will exist a lower limit to the defect size that yields detectable image contrast.

The quantities γ_D and β cannot be effectively predetermined; hence, empirical guidelines on defect detectability must firstly be obtained for typical defect/matrix systems, and then approximate scaling effects can be predicted using Eq.(12). Preliminary studies on inclusions in silicon nitride indicate that inclusions containing high atomic number elements (e.g. W, Fe) are readily detected using microfocus systems, at the smallest sizes of interest (~25μm). The detectability of inclusions with comparable atomic numbers to the matrix, such as Si and SiC, voids and cracks is less satisfactory; although, the detection limits that can be achieved with image enhancement capabilities has yet to be ascertained. Similarly, the ability to distinguish different defect types has yet to be evaluated. Some information is clearly available in the contrast ΔI (Eq. 12), but the extent to which this provides a satisfactory classification remains to be determined. Another difficulty that must be surmounted concerns the ability to obtain the defect dimension normal to the surface . This dimension influences the contrast (Eqn. 12), but it is not likely to be separable from the effect of the defect type. Tomographic techniques are a more plausible probability; but again, their efficacy in components of complex shape has yet to be determined.

The nature of the probability function $\phi(a_{es}|a)$ pertinent to the x-ray method deserves brief mention. Since the method creates an image of the defect, the error is concerned both with the measurement of the dimensions

from the image, and the ability to obtain a three-dimensional image. The former represents a random error, and is probably Gaussian; while the latter is a systematic error related to the component geometry and its effect on accessability of the x-ray beam to the defect. The magnitudes of these errors are presently being evaluated.

Finally, it is instructive to cursorily explore the utility of the x-ray method for failure prediction in hot pressed silicon nitride. If Si inclusions $\lesssim 800\mu m$ cannot be discerned, (as the available information suggests) then, since Si inclusions $\gtrsim 150\mu m$ in diameter are potential critical defects (Fig. 5), it may be concluded that the x-ray method is incapable of estimating the dimensions of certain types of critical defects. The false-accept (or failure) probability for the x-ray method is thus identical to the probability of occurrence of Si inclusions, in the size range ~ 150 to $800\mu m$. The method has not, therefore, effected a substantial reduction in the false-accept probability, vis-a-vis its value without inspection. This result suggests that future x-ray development pertinent to silicon nitride should be devoted to enhancing the detectability of inclusions of this type.

Ultrasonics

The advances in ultrasonic defect characterization have been appreciable in recent years. It is now apparent that all of the bulk defects and most of the surface defects of concern in ceramics can be detected with the appropriate ultrasonic technique. However, much additional study is needed to determine how well the pertinent defect dimensions and the defect type can be characterized. The requisite defect detectability has been achieved by noting

that the amplitude of the ultrasonic wave scattered by the defect increases rapidly as the wavelength λ decreases, to $\sim 2\pi a/\lambda$. Detectability is thus inhanced by selecting frequencies (up to 200 MHz) in excess of those conventionally used for defect detection (up to ~20 MHz). It also appears that the acoustic impedance mismatch between the defect and the matrix is sufficient for most defects of interest (especially when the defect contains porosity wnich reduces its effective impedence) to permit the required detectability.

The background scattering (which often imposes a lower limit on defect detectabiity) is not a concern for bulk defects of critical size (~25μm) in fine-grained structural ceramics (hot pressed Si_3N_4, hot pressed and sintered SiC); because the grain scattering is minimal up to ~400 MHz. The background is a concern, however, for surface crack detectability. The background in this case is associated with the scattering from arrays of surface cracks introduced by surface grinding. Typical detectability limits are indicated in Fig. 8. On polished surfaces, the smallest cracks that can be introduced (60μm diameter) are easily detected (Fig. 8a); for surfaces ground with 30μm diamond particles, the smallest cracks that can be detected are~ 80μm in diameter; while, for rough ground surfaces, cracks smaller than ~120μm cannot be detected.

The specific ultrasonic methods for bulk and surface defects are different, but the principles are the same. Bulk defects are characterized using longitudinal and/or shear waves propagated directly into the component; preferably using a transducer array that permits rapid electronic scanning of

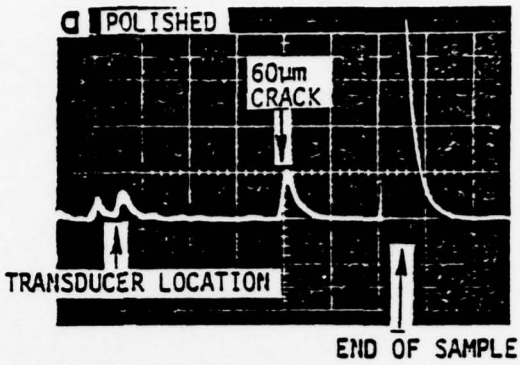
a POLISHED
60μm CRACK
TRANSDUCER LOCATION
END OF SAMPLE

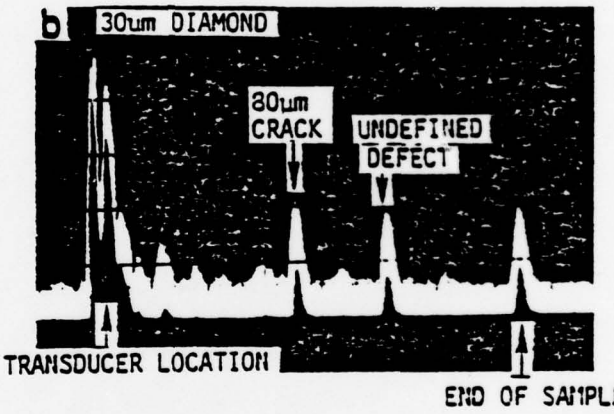
b 30μm DIAMOND
80μm CRACK
UNDEFINED DEFECT
TRANSDUCER LOCATION
END OF SAMPLE

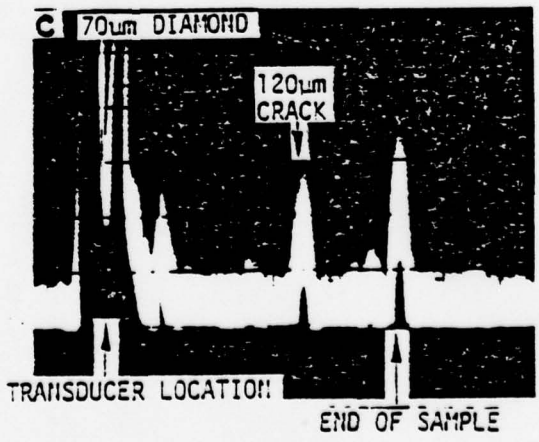
c 70μm DIAMOND
120μm CRACK
TRANSDUCER LOCATION
END OF SAMPLE

Figure 8

components, through a ceramic buffer contoured to match the component. Alternatively, a traversable transducer focused through a liquid metal medium may be employed. Surface cracks are characterized using surface waves, which can be excited on the component using ceramic waveguides and a fluid or polymeric couplant. Additional studies are needed, however, to design optimum transducer configurations.

The ultimate approach for ultrasonic defect characterization in ceramics remains to be developed. However, present knowledge suggests the following sequence. Following an initial rapid scan to determine the location of defects, the defect type will be identified from the characteristics of the scattered signal at high frequencies (100-400 MHz). The signal in the time domain has very characteristic features, as indicated by comparing the void signal (Fig. 9a) with the signal from a WC inclusion (Fig. 9b). Additionally, the frequency domain (obtained using a fast Fourier transform) contains information characteristic of the defect type. Note, however, that the pertinent information can only be obtained experimentally if transducer response is subtracted, e.g. using an inverse filter. Finally, the frequency dependence of the scattered amplitude in the long wavelength limit ($\lambda \gtrsim 10a$), i.e. at between approximately 5 and 50 MHz, can be used to provide a unique measure of the volume of the defect (Fig. 10). The scattering model used to obtain this information has been well-substantiated experimentally, at least for defects of regular shape, (vis. generalized ellipsoids, surface cracks). The model indicates that the scattered amplitude A at low frequencies is given by;

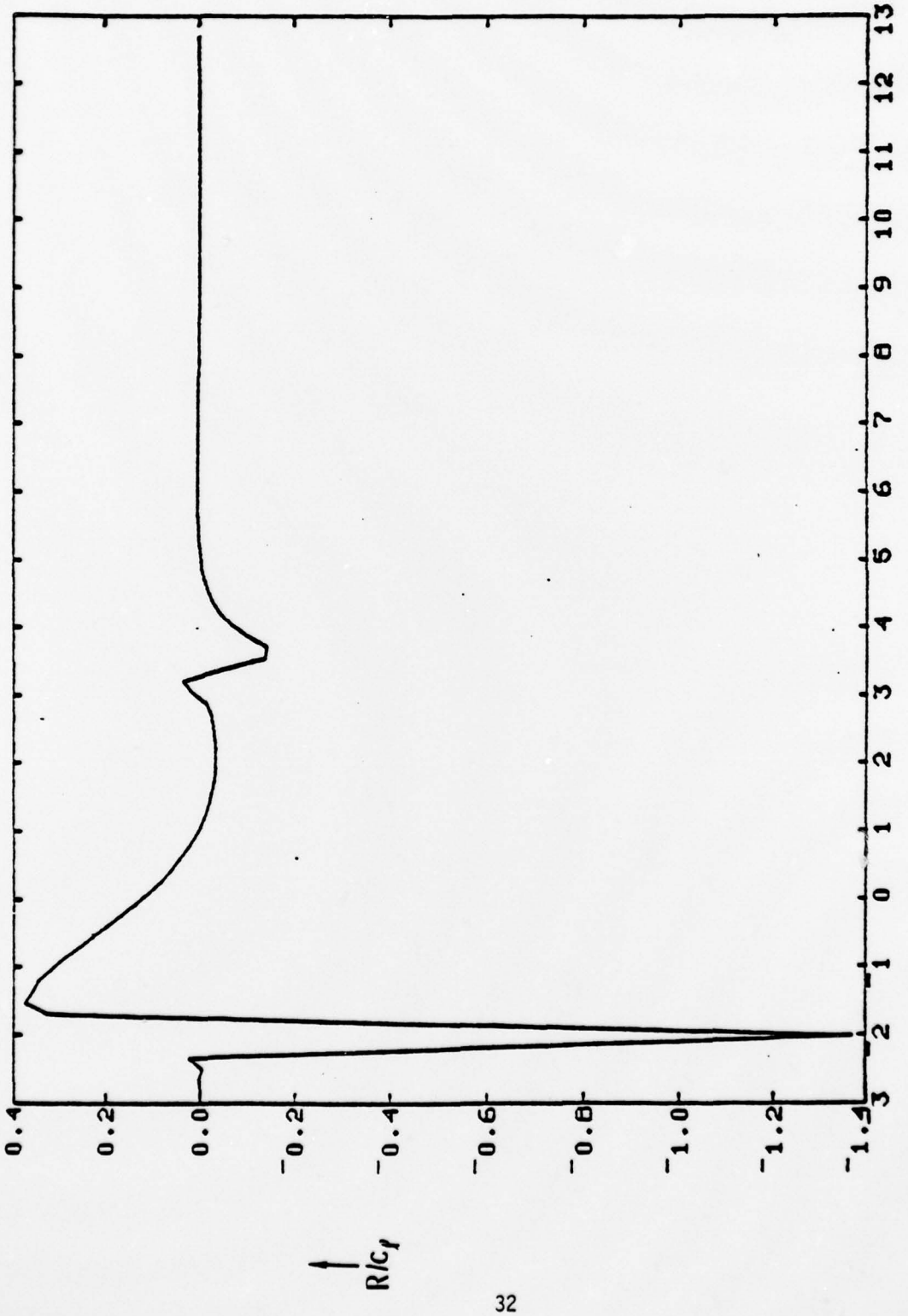

Fig. 9a R/c_ρ vs $c_\rho t/a$ FOR VOID IN Si_3N4.

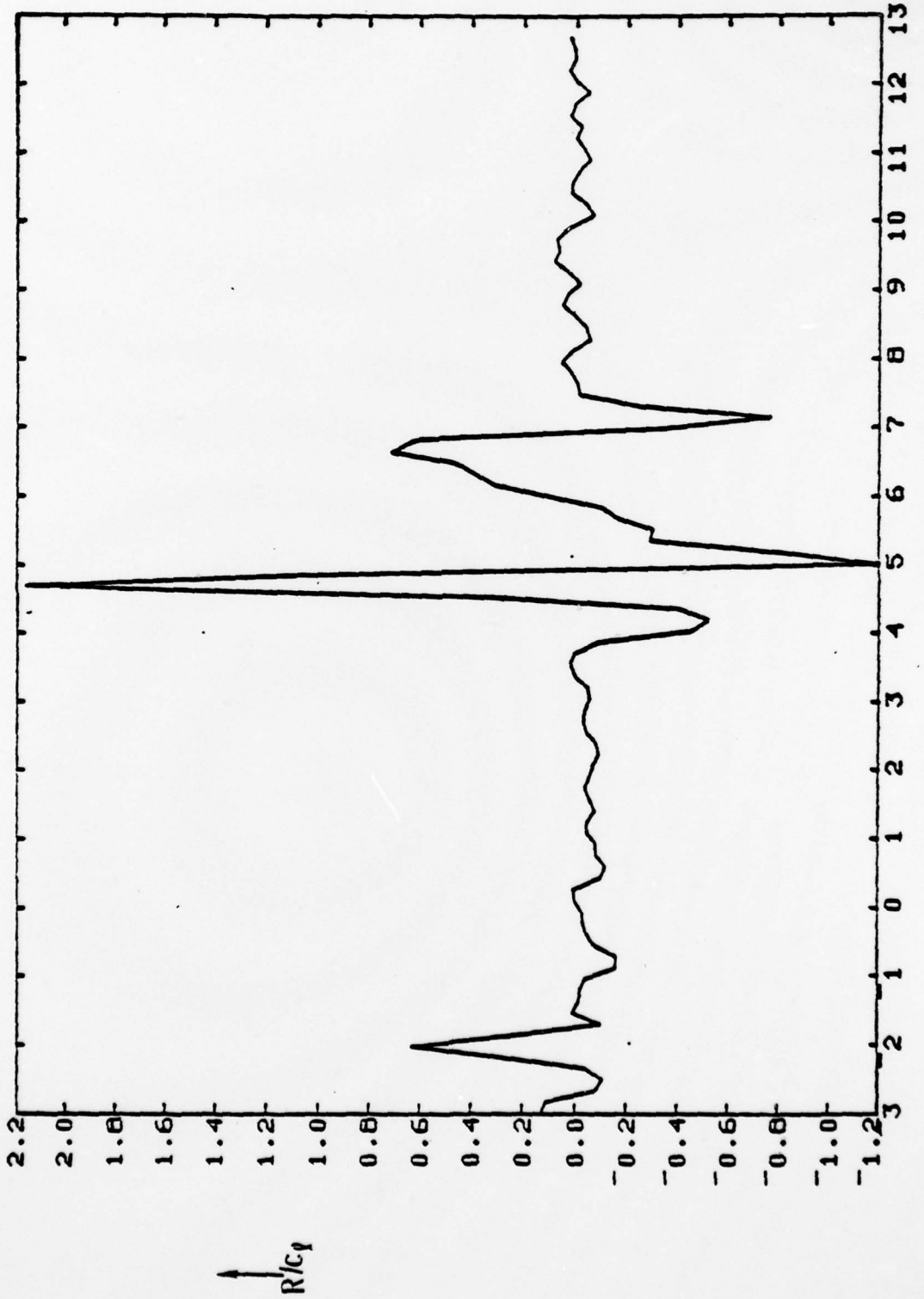

Figure 9b R/c_f vs $c_f t/a$ FOR A WC INCLUSION IN Si_3N_4

SC78-1484

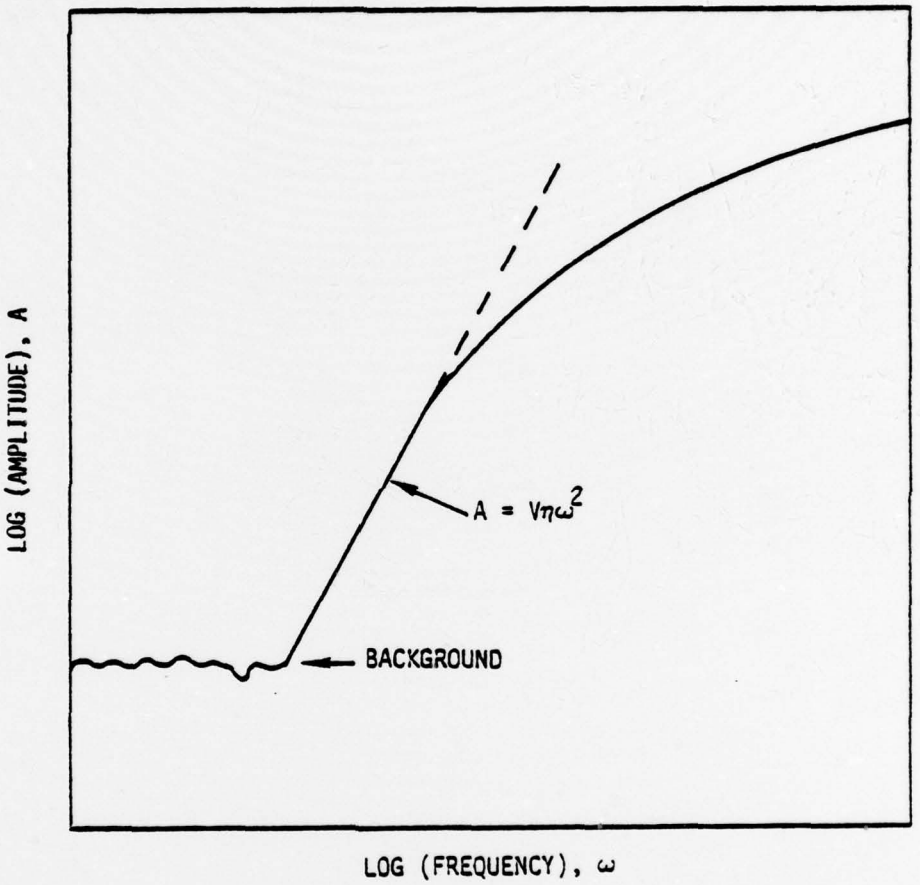

Figure 10

$$A = V\eta^2\omega^2 \tag{13}$$

where ω is the frequency, and η is a parameter that depends on the defect type and shape: for example, η for a spherical void is,

$$\eta = \left[1 + \frac{1+\nu}{7-2\nu} + \frac{10(1-2\nu)}{7-5\nu}\right]\left(\frac{1}{4\pi c_\ell^2}\right) \tag{14}$$

where ν is Poisson's ratio and c_ℓ is the longitudinal wave velocity in the matrix. Individual defect dimensions (a,b,c) and orientations can also be obtained from long wavelength data, if information is available for the same defect as several (up to 5) scattering angles. The viability of obtaining the quantity of information required to determine individual dimensions has yet to be demonstrated for a practical system.

The error associated with the estimate of the defect volume required for the reliability analysis has not been evaluated in detail for real defects; although the appropriate experiments are now underway. The errors are expected to be: a random error in the amplitude associated with the level of the background (probably Gaussian), a systematic error if the defect type is incorrectly assigned from the high frequency analysis, and an error (probably random in most cases) associated with the unknown orientation of the axes of the defect. These errors combine to yield the required function, $\phi(V_{es}|V)$.

SUMMARY

The general approach for quantitative failure prediction in ceramics using

nondestructive methods of defect characterization has been described. The current state of knowledge, as it impinges on the quantitative failure prediction issue, has been reviewed. The knowledge is incomplete, but considerable progress has been realized in the last two years toward attaining the requisite information. The next two years should see progress at an equal or more rapid rate, and the emergence of the first quantitative nondestructive failure prediction scheme for ceramics. At that juncture, it will be possible to select the best possible technique, or combination of techniques, pertinent to a specific material and component geometry. Substantial scope for the improvement of existing inspection techniques, and for the introduction of new techniques, will exist at that stage; such advances are to be encouraged, using the quantitative basis for technique comparison developed in this review.

BIBLIOGRAPHY

Interdisciplinary Program for Quantitative Flaw Definition, ARPA/AFML Contract F33615-74-C-5180. D.O. Thompson et al.

Ultrasonic Attenuation in Ceramics, A.G. Evans, B.R. Tittmann, L. Ahlberg, T.T. Khuri-Yakub and G.S. Kino, J. Appl. Phys. 49 (1978).

Failure Prediction in Structural Ceramics, A.G. Evans, G.S. Kino, R.T. Khuri-Yakub and B.R. Tittmann, Materials Eval., April 1977, p. 85.

Ultrasonic Detection of Surface Cracks in Ceramics, B.T. Khuri-Yakub, A.G. Evans, G.S. Kino and B.R. Tittmann, Science Center Report SC5064.3TR on ONR program N00014-76-C-0624.

Development of Nondestructive Testing Techniques for High Performance Ceramics, M.R. Baumgartner, R.H. Brockelman and P.M. Hanson, AMMRC Report, AMMRC Tr78-11.

Error Analysis of Failure Prediction, S.M. Wiederhorn, E.R. Fuller, J. Mandel and A.G. Evans, J. Amer. Cer. Soc. 59, (1976)

TECHNICAL REPORTS

Failure Prediction in Ceramics Using Ultrasonics, A. G. Evans, B. R. Tittmann and L. A. Ahlberg, 5064.1TR, March 1, 1976 - October 31, 1976.

Acoustic Surface Wave Scattering: The Detection of Surface Cracks in Ceramics, B. T. Khuri-Yakub, A. G. Evans, G. S. Kino, B. R. Tittmann, 5064.2TR, November 1, 1976 - November 30, 1977.